Validation of New Formulations for Propeller Analysis

J. Morgado,* M. Â. R. Silvestre,† and J. C. Páscoa‡
University of Beira Interior, 6200-001 Covilhã, Portugal

DOI: 10.2514/1.B35240

This paper reports the development of a new propeller design and analysis tool. JBLADE uses an improved version of blade element momentum that embeds a new model for the three-dimensional flow equilibrium. In addition, a new method for the prediction of the airfoil drag coefficient at a 90 deg angle of attack for a better poststall modeling is also presented. The software is developed as an open-source tool for the simulation of propellers and has the capability to estimate the performance of a given propeller geometry in design and offdesign operating conditions. The software allows the introduction of the blade geometry as an arbitrary number of sections. To validate the code, the propellers from NACA Technical Report 530 by Gray ("Wind-Tunnel Tests of Two Hamilton Standard Propellers Embodying Clark Y and NACA 16-Series Blade Sections," 1941) and NACA Technical Report 594 by Theodorsen et al. ("Characteristics of Six Propellers Including the High-Speed Range," 1937) were simulated and the results were checked against the experimental data and against those of other available codes. Although current development work is focused in the design of airship propellers, the long-term goal of the JBLADE development is to provide a user-friendly, accurate, and validated open-source code that can be used to design and optimize propellers for distinct applications.

Nomenclature

a_a	=	axial induction factor
a_t	=	tangential induction factor
B	=	number of blades
C_a	=	axial force coefficient
C_D	=	airfoil drag coefficient
C_L	=	airfoil lift coefficient
C_t	=	tangential force coefficient
c	=	blade local chord, m
c_p	=	power coefficient
c_t	=	thrust coefficient
D	=	propeller diameter, m
F	=	Prandtl's correction factor
L	=	lift force, N
P	=	power, W
Q	=	torque, N · m
R_{LE}	=	airfoil leading-edge radius
r	=	radius of blade element position, m
T	=	thrust, N
t	=	airfoil thickness
W	=	element relative velocity, m/s
W_a	=	element axial velocity, m/s
W_t	=	element tangential velocity, m/s
x/c	=	nondimensional x position
$(y/c)_{0.0125}$	=	nondimensional y position at x/c equal to 0.0125
α	=	angle of attack, deg
θ	=	incidence angle, deg
ρ	=	air density, kg/m^3
σ_r	=	local solidity ratio
ϕ	=	inflow angle, deg
Ω	=	rotation speed, rad/s

Presented as Papers 2013-4220 and 2013-4379 at the Aviation 2013, Los Angeles, CA, 12–14 August 2013; received 5 November 2013; revision received 15 July 2014; accepted for publication 16 July 2014; published online 14 October 2014.

*Ph.D. Student, Aerospace Sciences Department, Rua Marquês D'Ávila e Bolama. Student Member AIAA (Corresponding Author).

†Assistant Professor, Aerospace Sciences Department, Rua Marquês D'Ávila e Bolama. Senior Member AIAA.

‡Assistant Professor, Electromechanics Department, Rua Marquês D'Ávila e Bolama.

I. Introduction

THE problems caused by growth in the transportation sector, e.g., the rise of fuel consumption and cost, as well as pollution and consequent climate change led to a reconsideration of the transportation systems by the most economically advanced nations [1]. Nowadays, despite all technologic developments, as we proceed into the 21st century, we may be about to witness the return of slower air transport as a means of increasing energy efficiency and business profitability.

Slowing down aircraft can take us toward the airship. After an initial development until the 1930s, the airships were only considered as a mere curiosity. At their peak, in the late 1930s, airships were unrivaled in transoceanic transportation. Nowadays, they can be used effectively as platforms for different purposes [2–5], especially activities that require long endurance or hovering for a long time.

In Europe, the development of the new airships is also being supported by the European Union through the Multibody Concept for Advanced Airship for Transport (MAAT [6]) project. This collaborative project aims to develop a heavy lift cruiser–feeder airship system in order to provide middle- and long-range transport for passengers and goods. The MAAT system is composed of the cruiser and the feeder modules. The feeder is a vertical takeoff and landing system that ensures the connection between the ground and the cruiser. It can go up and down by control of the buoyancy force and displace horizontally to join to the cruiser. The cruiser is conceived to move mostly in a horizontal way at high altitude. Since the MAAT project has the objective of operating an airship at stratospheric altitudes, propellers are a valid option for the airships' propulsion [7].

An airship propeller must be efficient in thrust per unit of power in the hovering flight condition, and it needs to have a high propulsive efficiency in cruise flight. The design of a propeller for an altitude of about 15 km can itself be difficult [8], but it is crucial to develop a numerical tool that allows the design and optimization of MAAT airship propellers over the broad operating conditions in which these will operate. To maximize the propeller performance over the intended extreme flight envelope, it is required to optimize the shape and structure of the propeller as well as the coupling with its respective motor sets. The optimization process is based on the analysis and comparison of numerous designs and their relative merits. This can only be achieved in a practical way with low-computational-cost numerical tools.

The first developments related to the theory of propellers occurred in the 19th century with Rankine [9] and Froude [10] through a work focused on marine propellers. Later, Drzewiecki [11] presented the blade element theory. However, he did not take into account the effect

of the propeller-induced velocity on each element. In 1919, Betz and Prandtl [12] stated that the load distribution for lightly loaded propellers with minimum energy loss is such that the shed vorticity forms regular helicoidal vortex sheets moving backward, undeformed behind the propeller. Thus, the induced losses of the propellers will be minimized if the propeller slipstream has a constant axial velocity and if each cross section of the slipstream rotates around the propeller axis like a rigid disk [13].

Prandtl (as cited by Glauert [14]) found an approximation to the flow around helicoidal vortex sheets, which is good if the advance ratio is small and improves as the number of blades increases. The approximation presented by Prandtl is still applied in simple mathematical codes. Later, Goldstein [15] found a solution for the potential field and the distribution of circulation for propellers with small advance ratios. Theodorsen [16], through his study on the vortex system in the far field of the propeller, concluded that Goldstein's solution [15] for the field of a helicoidal vortex sheet remains valid, even for moderate/highly loaded propellers. In 1980, Larrabee [17] analyzed the steady air loads on the propeller and presented a practical design theory for minimum induced loss propellers. This method is a combination between momentum theory, blade element theory, and vortex theory. Later on, Adkins and Liebeck [18] presented improvements with small-angle approximations and light-load approximations, overcoming the restrictions in the method developed by Larrabee [17].

Presently, there are several codes to design propellers and predict their performance. These codes typically use the blade element momentum (BEM) theory together with two-dimensional airfoil data. However, they are somewhat inconsistent in accurately predicting the propeller thrust and power [19] over a significant portion of the propeller's speed envelope. Part of the inaccuracy comes from the classical BEM assumption that the velocity induced by one element has no effect on its neighboring blade elements [20]. This is dealt with in the present work by modifying the classical BEM theory with the introduction of a new three-dimensional (3-D) flow equilibrium formulation that redistributes the tangential induced velocity. Another part of the failure to accurately compute the propeller performance results from the deep-stall angles of attack that the blade elements can achieve during their normal operation, since the experimental data from wind-tunnel measurements are only available over a limited interval of angles of attack [21,22], commonly between -5 to $+20$ deg, and the airfoil performance prediction codes do not work in this full range of high angles of attack.

Although some analytical and experimental studies [23–27] have tried to fully understand the effect of the complex 3-D flow physics of rotary wings on the blade airfoils' aerodynamics, there is still a need to extend the common available airfoil data to the full interval of angles of attack involved in blade operations in order to obtain a closer prediction of airfoil performance.

II. Methodology

A. Classical Blade Element Momentum Theory

To model the propeller, the blade is divided into a set of blade elements. Each blade element is a discrete rotating wing (see Fig. 1) [28]. The blade element relative velocity and respective inflow angle are computed through the axial and tangential velocity components. The axial velocity results from the sum of the propeller airspeed to the induced axial velocity at the propeller disk. The tangential velocity results from the sum of the velocity of the element due to the propeller rotation, with the induced tangential velocity. The induced velocity components are determined from the momentum theory, for the annulus swept by the rotating blade element, and used to calculate the angle of attack as the difference between ϕ and θ. With α, the element's lift and drag coefficients can be determined. With these coefficients, the axial and tangential force coefficients are obtained according to the local θ:

$$C_a = C_L \cos\phi - C_D \sin\phi \tag{1}$$

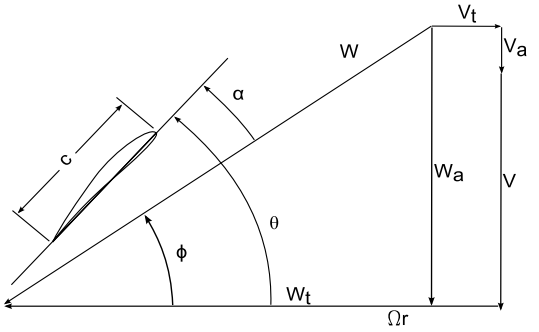

Fig. 1 Blade geometry and velocity triangle at an arbitrary radius blade position [28].

$$C_t = C_L \sin\phi + C_D \cos\phi \tag{2}$$

To describe the overall propeller performance, the forces are obtained from the force coefficients according to

$$F_x = \frac{1}{2}\rho W^2 c C_x \tag{3}$$

The total thrust and torque of the propeller are calculated from

$$T = B\int_{R_{\text{root}}}^{R_{\text{tip}}} F_a \,\mathrm{d}r \tag{4}$$

$$Q = B\int_{R_{\text{root}}}^{R_{\text{tip}}} F_t r \,\mathrm{d}r \tag{5}$$

With the total torque from Eq. (5), the necessary shaft power is obtained:

$$P = \Omega Q \tag{6}$$

and dimensionless thrust and power coefficients are calculated from their definitions:

$$c_t = \frac{T}{\rho n^2 D^4} \tag{7}$$

$$c_p = \frac{P}{\rho n^3 D^5} \tag{8}$$

When the advance ratio is defined as presented in Eq. (9), the propeller efficiency is computed through Eq. (10):

$$J = \frac{v}{nD} \tag{9}$$

$$\eta = \frac{c_t}{c_p} J \tag{10}$$

The iteration variables of the classical BEM method are the axial and tangential induction factors, defined from the induced velocity components as

$$a_a = \frac{W_a - V}{V} \tag{11}$$

$$a_t = \frac{\Omega r - W_t}{\Omega r} \tag{12}$$

and by including results from momentum theory

$$a_a = \left(\frac{4F\sin^2\phi}{\sigma C_a} - 1\right)^{-1} \tag{13}$$

$$a_t = \left(\frac{4F\sin\phi\cos\phi}{\sigma C_t} + 1\right)^{-1} \tag{14}$$

where σ_r is the ratio of the blade element area to the annulus sweep by the element in its rotation, and it is defined by Eq. (15):

$$\sigma_r = \frac{cB}{2\pi r} \tag{15}$$

In Eqs. (13) and (14), F compensates for the amount of work that can actually be performed by the element according to its proximity to the blade's root or tip. If the element is at the blade tip, its contribution will be zero. F is estimated according to Eq. (16) in the 3-D corrections model.

To compute ϕ, the induction factors a_a and a_t must be known. An arbitrary value is assigned for both axial and tangential induction factors for the first iteration. The iteration is repeated for all blade elements. Thus, with lift and drag coefficients for the angle of attack, the induction factors are updated and compared to the ones from the previous iteration. As soon as the difference is below the convergence criteria defined by the user, the iteration stops and the next blade element is computed.

B. Three-Dimensional Corrections Model

During each iteration, the code also takes into account the losses caused by tip and root vortices. These corrections, previously described by Prandtl [14], are modeled by

$$F = \frac{2}{\pi}a\cos(e^{-f}) \tag{16}$$

where

$$f_{\text{root}} = \frac{B}{2}\left(1 + \frac{R_{\text{root}}}{r}\right)\frac{1}{g} \tag{17}$$

$$g_{\text{root}} = \frac{R_{\text{root}}}{r}\tan\phi \tag{18}$$

or

$$f_{\text{tip}} = \frac{B}{2}\left(1 - \frac{r}{R_{\text{tip}}}\right)\frac{1}{g} \tag{19}$$

$$g_{\text{tip}} = \frac{r}{R_{\text{tip}}}\tan\phi \tag{20}$$

C. New Three-Dimensional Flow Equilibrium Model

The theoretical formulation presented in Secs. II.A. and II.B. assumes that the flow in the propeller annulus is two-dimensional, meaning that radial movement of the flow is neglected. But for such a condition, tridimensional equilibrium [29] must exist. Furthermore, the classical BEM formulation assumes that neighboring blade-element-induced velocities are independent, which lacks physical reasoning [20]. In JBLADE, this issue is addressed by a new model based on 3-D flow equilibrium:

$$W_a\frac{\partial W_a}{\partial r} + W_t\frac{\partial W_t}{\partial r} + \frac{W_t^2}{r} = 0 \tag{21}$$

The case where W_a is maintained constant across the propeller annulus reduces Eq. (21) to

$$\frac{\mathrm{d}W_t}{\mathrm{d}r} = -\frac{W_t}{r} \Leftrightarrow W_t r = \text{const.} \tag{22}$$

In this case, the whirl varies inversely with the radius, which is best known as the free vortex condition. Although this differs substantially from the ordinary BEM approach, where the momentum theory applied to the tangential velocity induction totally disregards the neighbor elements to determine the element's V_t, it makes sense when one considers that, from far upstream down to the propeller disk, the flow should be isentropic or close to irrotational, thus respecting the free vortex condition. To implement this equilibrium condition, in the first iteration, the force coefficients are computed assuming no tangential induction factor, which means that $a_t = 0$. The mass flow rate at annulus element i is calculated as

$$\dot{m}_i = 2\rho W_a \pi r\,\mathrm{d}r \tag{23}$$

and

$$\dot{m}_{\text{total}} = \int_{r_{\text{root}}}^{r_{\text{tip}}} \dot{m}_i \tag{24}$$

To satisfy the momentum conservation, the total propeller torque will be the result of a free vortex-induced tangential velocity profile with an average axial velocity $\bar{W}_a$ across the propeller disk. A reference value of tangential induced velocity is used that corresponds to that at 75% of the blade radius position, $V_{t_{75}}$. The average axial velocity is

$$\bar{W}_a = \frac{\dot{m}_{\text{total}}}{\pi\rho R^2} \tag{25}$$

According to Eq. (26), at a given element, V_t is

$$V_t = \frac{0.75RV_{t_{75}}}{r} \tag{26}$$

$$Q = \int 4\pi\rho\bar{W}_a V_t r\,\mathrm{d}r \tag{27}$$

Thus, replacing Eqs. (25) and (26) in Eq. (27) and solving for $V_{t_{75}}$,

$$V_{t_{75}} = \frac{2}{3}\frac{Q}{\pi\rho\bar{W}_a R(R_{\text{tip}}^2 - R_{\text{root}}^2)} \tag{28}$$

The tangential induction factor can be updated, and the coefficients will be calculated again with the updated tangential induction factor:

$$a_t = \frac{V_t}{\Omega r} \tag{29}$$

The tangential velocity along an APC 10×7 in. slow flyer blade radius was plotted together with computational fluid dynamics (CFD) data and original BEM formulation in order to validate the new proposed model.

It is seen in Fig. 2 that the 3-D equilibrium hypothesis is a fair approximation with reality, considering that the CFD results show the real trend. The weakness of the BEM is also clear with respect to the tangential induction, since each annular element of the disk has no relation to its neighbor elements, allowing discontinuities in the tangential induction profile. The underprediction of tangential velocity in the BEM simulation is related to the lower power coefficient that results from its formulation in this static thrust condition.

To check the validity of the 3-D equilibrium hypothesis, a CFD simulation of the actual 3-D rotating propeller was performed. The propeller geometry details can be found in the University of Illinois Urbana–Champaign propeller data site [30]. Regarding the CFD simulation of the propeller, the commercial package Fluent® [31] is used with the k-w shear-stress transport turbulence model [32].

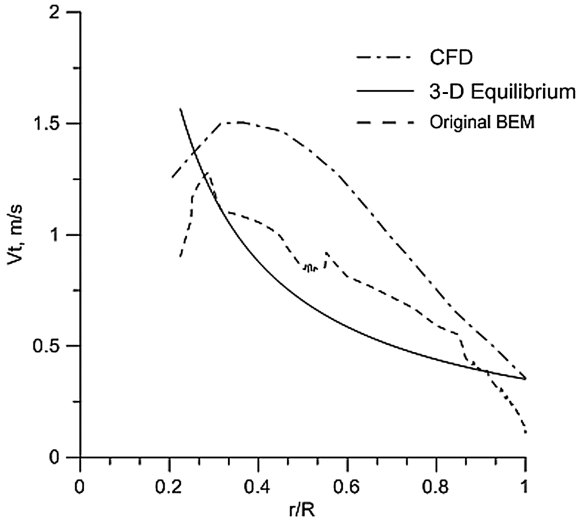

Fig. 2 Tangential velocity distribution along an APC 10 × 7 in. [30] blade radius at 1 m behind the propeller plane for CFD, original BEM formulation, and new proposed 3-D flow equilibrium model.

The hybrid mesh contains 2.5×10^6 points, and it is used as an implicit integration of the incompressible Navier–Stokes equation coupled with turbulent transport equations. Furthermore, the SIMPLE algorithm is used for pressure–velocity coupling. To consider the rotation of the propeller, a multiple reference frame approach is adopted. Thus, the computational domain is divided into two regions: the internal domain, which covers the propeller and is rotating at 3000 rpm; and the external domain, which is considered to be stationary. The second-order upwind scheme is used for the convection terms, whereas the diffusion terms are discretized using a central scheme. The convergence of the numerical solution is controlled and observed by assigning suitable underrelaxation of the transport equations so that the relative numerical error of the solution drops below 1.0^{-7}.

D. New Method for C_{D90} Prediction

During the extrapolation process, one of the aspects with major weight, as referred to by Montgomerie [21], is the airfoil drag coefficient at an angle of attack of 90 deg. The developments to predict the drag coefficient at 90 deg began with Gault [33], who presented the low-speed stalling characteristics of airfoils and correlated them with a single specific upper thickness coordinate at $x/c = 0.0125$. The results presented by Gault are restricted to airfoils without high-lift devices and to airfoils with aerodynamically smooth surfaces, and he considered the Reynolds number influence on airfoil stalling characteristics. Later, in 1995, Montgmorie [21] presented two different methods to predict the value of the drag coefficient and its distribution along a wind turbine blade. The first method considers a constant drag coefficient distribution along the entire blade and represents the most widely used method by manufacturers. The second method consists of a curvilinear distribution of the drag coefficient at 90 deg.

Initially, the method described by Montgmorie [34] was used in JBLADE, but the authors found that different extrapolated 360 deg polars will lead to significant differences in final predicted power and thrust forces for the same propeller.

In this new proposed method, C_{D90} is correlated with the airfoil leading-edge radius. The leading-edge radius of an arbitrary airfoil is calculated using an approximation by the least-square method on its set of contour coordinates. For a NACA four-digit-series airfoil, it is possible to calculate the leading-edge radius through Eq. (30) [35]:

$$R_{\mathrm{LE}} = 1.109t^2 \tag{30}$$

The leading-edge radius was calculated for different NACA airfoils, and the results are presented in Table 1.

The greatest difference occurs for an airfoil with 9% thickness, and it is 3.75%, which is a reasonably low value. The leading-edge radius of specific airfoils was then calculated and plotted against their experimentally measured values of drag coefficient at 90 deg, as presented in Fig. 3.

The linear correlation that was found to fit the data is shown in Eq. (31):

$$C_{D_{90}} = 2.0772 - 3.978\mathrm{LE}_{\mathrm{Radius}} \tag{31}$$

In addition, an improvement to the fitting previously presented by Timmer [36] was implemented. The airfoil y coordinate at $x/c = 0.0125$ for more airfoils (see Table 2 [22,36–39]) was calculated, and airfoils were added to the originally considered database.

The comparison between new and original correlations can be observed in Fig. 4. This new correlation was also implemented in the JBLADE [40] software, providing a second option for the calculation of C_{D90}, and consequently for airfoil polar extrapolation.

The new fit obtained with the y coordinate at $x/c = 0.0125$ is given by

$$C_{D_{90}} = 2.086 - 4.6313(y/c)_{0.0125} \tag{32}$$

E. Poststall Model

The rotational motion of the blade affects the element's boundary layer such that the airfoil stall shifts to higher angles of attack. So, a correction for the mentioned problem is also implemented in JBLADE. The correction is based on the work of Corrigan and Schillings [41] and is presented in Eq. (33). This model is based on the local solidity ratio and relates the stall delay to the ratio of the local blade chord to radial position:

$$c_{\mathrm{rot}(\alpha+\Delta\alpha)} = c_{\text{non-rot}}\left(\frac{\mathrm{d}c_l}{\mathrm{d}\alpha}\Delta\alpha\right) \tag{33}$$

where

$$\Delta\alpha = \left[\left(\frac{K(\frac{c}{r})}{0.136}\right)^n - 1\right](\alpha_{C_{L_{\max}}} - \alpha_{C_{L_0}})$$

The separation point is related with the velocity gradient K through Eq. (34):

$$\left(\frac{c}{r}\right) = 0.1517\ \mathrm{K}^{-1.084} \tag{34}$$

F. JBLADE Software

To implement and verify the improvements presented in this paper, the proposed models were implemented in JBLADE software. JBLADE [40] is being developed by the authors as a numerical open-source propeller design and analysis code written in C++/QML programming language [42]. The code is based on QBLADE [43,44]

Table 1 Leading-edge (LE) radius calculations and errors due to least-square method approximation

Airfoil name	LE radius with Eq. (30)	LE radius with least-square method	Error, %
NACA 0012	0.01597	0.01596	0.06
NACA 0015	0.02495	0.02472	0.93
NACA 0018	0.03593	0.03525	1.93
NACA 4409	0.00898	0.00933	3.75
NACA 4412	0.01597	0.01629	1.96
NACA 4415	0.02495	0.02511	0.64
NACA 4418	0.03593	0.03597	0.11

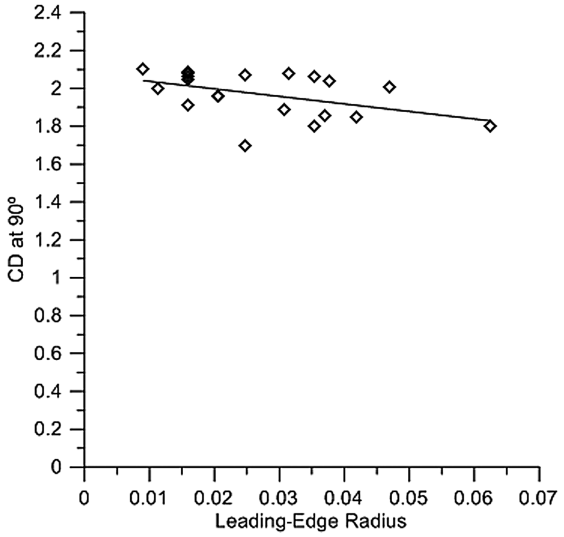

Fig. 3 Measured airfoil drag coefficient at 90 deg angle of attack vs airfoil leading-edge radius.

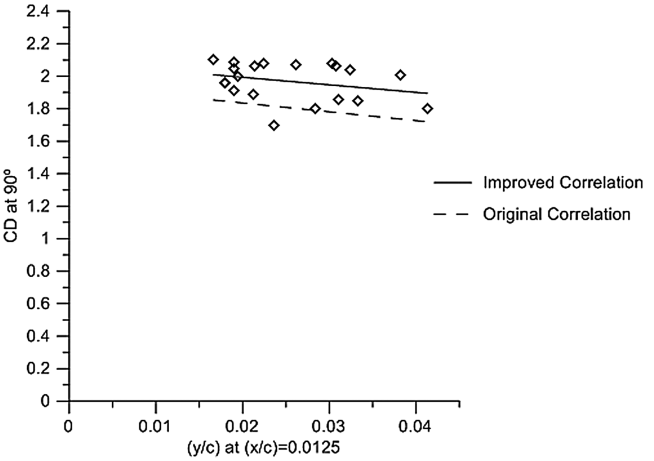

Fig. 4 Comparison between original and improved correlations based on method described by Timmer [36].

and XFLR5 [45] codes. It uses the classical blade element momentum theory, modified to account for three-dimensional flow equilibrium. Its methodology and theoretical formulation for propeller analysis are presented herein. The code can estimate the performance curves of a given design for offdesign analysis. The software has a graphical user interface, making easier to build and analyze the propeller simulations. The long-term goal of the JBLADE is to provide a user-friendly, accurate, and validated open-source code that can be used to design and optimize a variety of propellers.

The airfoil performance figures needed for the blades simulation come from QBLADE's coupling with the open-source code XFOIL [46]. This integration, which is also being improved, allows the fast design of custom airfoils and computation of their lift and drag polars. In addition, it is possible to import extrapolated, wind-tunnel, or CFD airfoil polars in the propeller simulation.

III. Results and Discussion

A. Test Cases

To validate JBLADE code and verify the reliability of the new developed models, the propellers described in NACA Technical Reports 594 [47] and 530 [48] were simulated.

The propellers have the Clark Y airfoil, with variable thickness along the blade span sections. Details of the propeller geometries and data for the different blade pitch angles can be seen in Figs. 5 and 6.

The propeller presented in Fig. 5 corresponds to the configuration named "nose 6–propeller c" from NACA Technical Report 594 [47], whereas the geometry in Fig. 6 corresponds to propeller 6267A-18 from NACA Technical Report 530 [48].

The airfoil polars were obtained with the XFOIL module. Each section of the blade has specific Reynolds and Mach numbers for which the airfoils were previously simulated. These polars were extrapolated such that the lift and drag coefficients became available for higher angles of attack. The geometries presented on the left sides of Figs. 5 and 6 were replicated in JBLADE, and the corresponding airfoil for each blade section was used, obtaining the propeller represented on the right sides of Figs. 5 and 6. The blade pitch angle was adjusted to the given angle at 75% of the radius, and the propeller performance was computed.

To correctly replicate the geometries previously presented, the authors have researched how the pitch angle was measured in the NACA reports [47,48]. However, the NACA reports do not give a clear indication about how the blade angle was measured at each radial position. Analyzing the two common reference lines (see Fig. 7), it was concluded that NACA tests refer to the lower surface of the blade, which was the usual practice at that time. Analyzing the difference on a Clark Y airfoil having 12% thickness, it becomes

$$\theta_{\text{Axis}} - \theta_{\text{LowerSurface}} = 2 \text{ deg} \tag{35}$$

Table 2 Maximum drag coefficient measured and calculated by two methods for a set of airfoils

Airfoil name	Reference	Measured C_{D90}	Calculated C_{D90} with $\text{LE}_{\text{Radius}}$	Calculated C_{D90} with $y/c_{(x/c=0.0125)}$
DU 91-W2-250	Timmer [36]	1.859	1.9302	1.9424
DU-97-W-300	Timmer [36]	1.845	1.9107	1.9319
FX 84-W-127	Massini et al. [37]	2.000	2.0325	1.9959
FX 84-W-218	Massini et al. [37]	2.040	1.9274	1.9359
LS-417	Timmer [36]	1.887	1.9545	1.9874
LS-421-MOD	Massini et al. [37]	2.010	1.8903	1.9088
NACA 0012	Lindenburg [22]	2.090	2.0141	1.9983
NACA 0012	Massini et al. [37]	2.050	2.0141	1.9983
NACA 0012	Timmer [36]	1.914	2.0141	1.9983
NACA 0015	Miley [38]	1.700	1.9779	1.9766
NACA 0018	Timmer [36]	1.800	1.9368	1.9544
NACA 4409	Ostowari and Naik [39]	2.100	2.0411	2.0089
NACA 4412	Ostowari and Naik [39]	2.060	2.0140	1.9868
NACA 4415	Ostowari and Naik [39]	2.068	1.9792	1.9652
NACA 4418	Ostowari and Naik [39]	2.060	1.9367	1.9433
NACA 23012	Massini et al. [37]	2.082	2.0140	1.9820
NACA 23017	Massini et al. [37]	2.078	1.9517	1.9453
NACA 23024	Lindenburg [22]	1.798	1.8283	1.8948
NACA 63-215	Lindenburg [22]	1.959	1.9954	2.0030

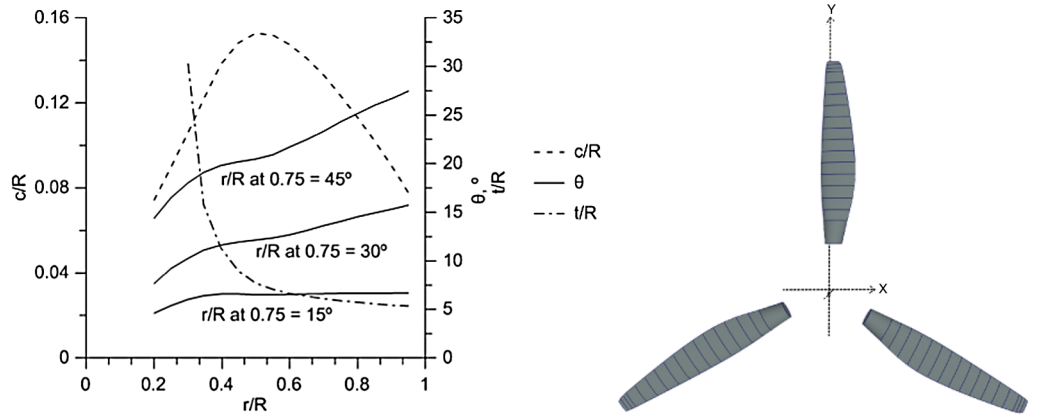

Fig. 5 Propeller geometry presented in NACA technical report 594 [47] and its shape after introduced in JBLADE. The propeller has three blades and a diameter of 3.054 m.

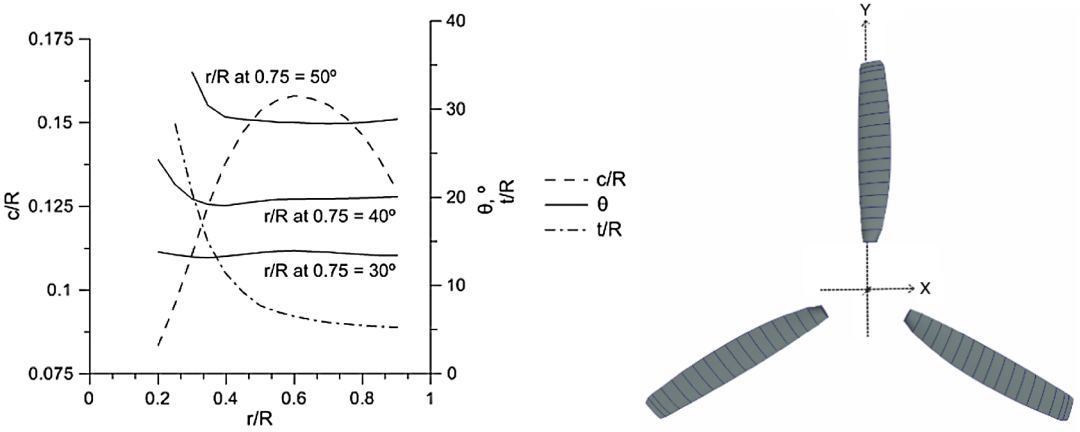

Fig. 6 Propeller geometry presented in NACA technical report 530 [48] and its shape after introduced in JBLADE. The propeller has three blades and a diameter of 3.073 m.

Since JBLADE uses the axis of the airfoil as the reference for the angle measurements, those 2 deg were added to the geometries found in the NACA reports [47,48].

B. Propeller Simulation

To simulate the propeller in JBLADE, the number of points required to define the airfoil coordinates in order to optimize XFOIL numerical accuracy was first studied. In Fig. 8 are presented the different polars obtained with different numbers of points in the airfoil definition. It was concluded that, for more than 200 points, XFOIL does not show a significant difference in the airfoil polars. So, each airfoil should be redefined in order to have 200 points.

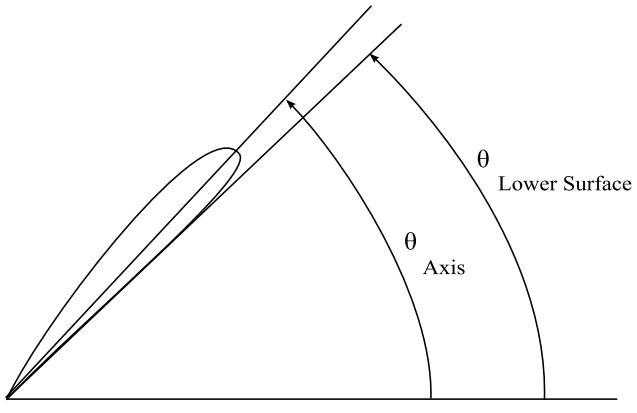

Fig. 7 Two possible references for blade pitch angle.

To validate the computations for a wide range of advance ratios, independent simulations for small and large advance ratios were computed and compared with the previously calculated curve using an average distribution of Reynolds and Mach numbers along the blade (see Fig. 9). For each of the blade's defining sections, the average Reynolds and Mach numbers were set as the mean values corresponding to half the advance ratio that corresponded to the propeller operating conditions used to collect the experimental data. The "VMIN" points were obtained with the distribution of Reynolds and Mach numbers for a low-airspeed operating condition. The propeller rotational speed was constant at 1800 rpm. The airfoil polars were calculated using those Reynolds and Mach numbers, and the propeller performance was only analyzed for that specified speed. The "VMAX" points were obtained with same procedure but for an airspeed close to the highest-advance-ratio zero thrust condition. The "COMPUTED" curves were calculated with the Reynolds and Mach number distributions collected for the intermediate velocities close to the maximum efficiency ("VMED" points). These averaged Reynolds and Mach number distributions (VMED) correspond to the intermediate advance ratio corresponding to that particular pitch setting, and they allow a close approximation for the full range of advance ratios, simplifying the simulation.

The history of the improvements on the theoretical formulation of JBLADE can be seen in Fig. 10 [49] and Fig. 11. "JBLADE$C_{D9} = 1.4$" was the initial formulation, as it was incorporated in QBLADE for wind turbines but extended here to simulate propellers. The dashed lines were obtained with a constant value of drag coefficient as suggested by Montgomorie [21] in his first method. According to this method, the value of $C_{D90} = 1.4$ was used for all airfoils from root to tip. "BEM–improved 360 polar"

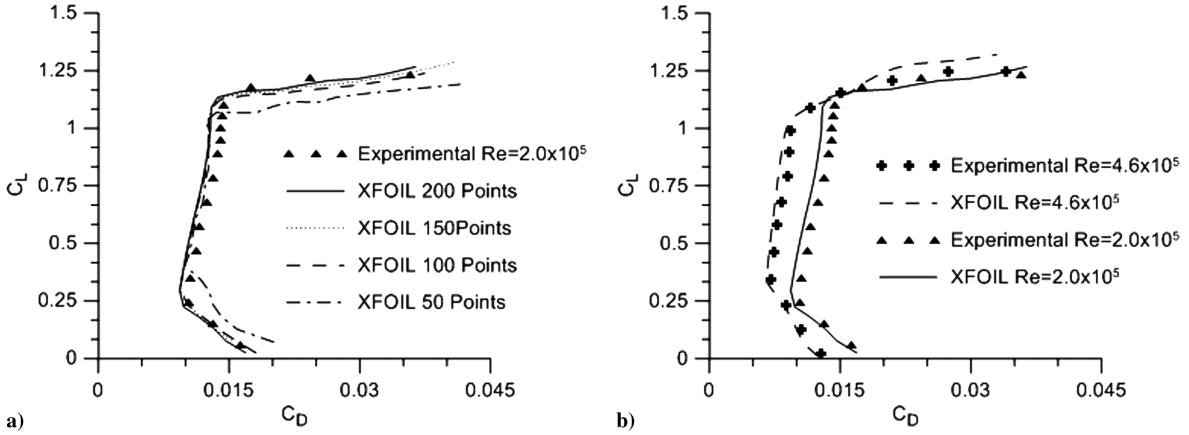

Fig. 8 Representations of a) validation of polar calculation using different number of points to define an airfoil in XFOIL; and b) comparison between XFOIL and experimental studies [49] for E387 airfoil and different Reynolds numbers.

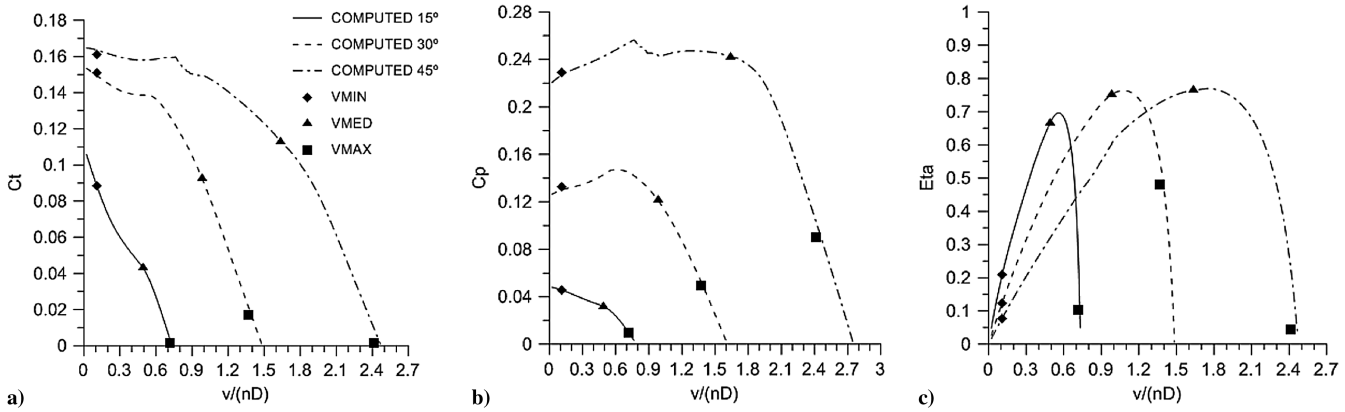

Fig. 9 Validation of calculations using a distribution of averaged Reynolds and Mach numbers along the blade: a) thrust coefficient, b) power coefficient, and c) propeller efficiency.

corresponds to the modified 360 deg range of angle-of-attack polar model improvement described in Sec. II.D. The solid lines were obtained with the presently proposed methods, where C_{D90} is correlated with the leading-edge radius. This method modifies the value of drag coefficient at 90 deg to a more reasonable value, and consequently changes the extrapolated 360 deg angle-of-attack airfoil drag coefficient polar. "JBLADE$C_{D9} = 2.2$" also represents a constant C_{D90} along the blade. It is seen that the C_{D90} and the complete 360 deg angle-of-attack range airfoil polars play an important role in the predicted performance, with a visible improvement in the thrust and power coefficients at low advance ratios and a slight underprediction at high advance ratios for the thrust coefficient.

The "mod. BEM" curve in Fig. 11 corresponds to the modification of the classical BEM with the 3-D equilibrium described in Sec. II.C, resulting in significant improvements throughout the complete advance ratio range. "Mod. BEM + poststall" includes the poststall model described in Sec. II.E and corresponds to the final formulation used in the simulations thereafter.

C. Results

Figure 12 shows that JBLADE closely predicts the thrust coefficient; however, the power coefficient is significantly underpredicted at low advance ratios and slightly overestimated in the higher end. It was found in the first case that the cause may be attributed to the airfoil's 360 deg angle-of-attack range airfoil polar misrepresentation just above the stall since that, at the lower advance ratios together with high pitch angles, a significant portion of the blade root is well into deep-stall angles of attack and the airfoil performance is obtained from XFOIL predictions that are not accurate for poststall regimes. The propeller efficiency is thus overpredicted in this region. The advance ratio for the maximum efficiency closely matches the experimental values, but the maximum

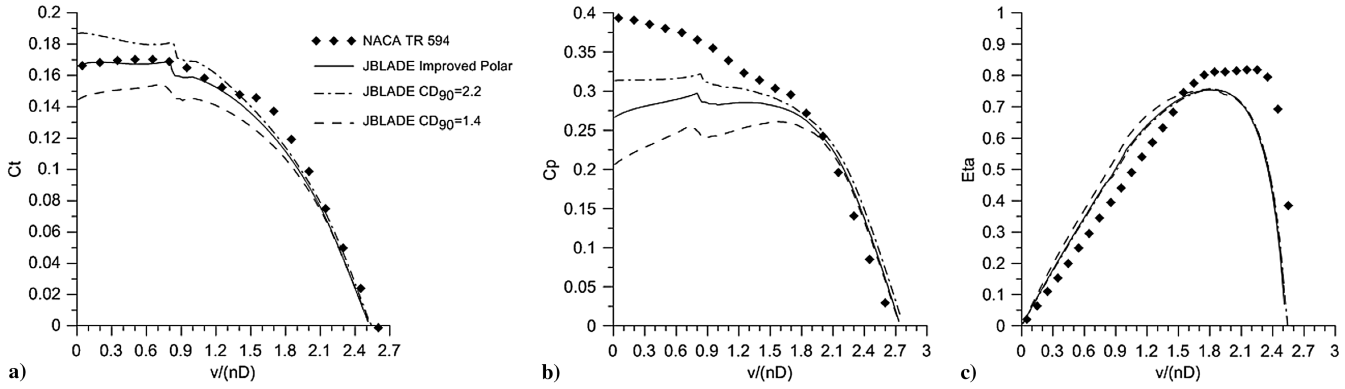

Fig. 10 Influence of the 360 polars extrapolation in the propeller performance.

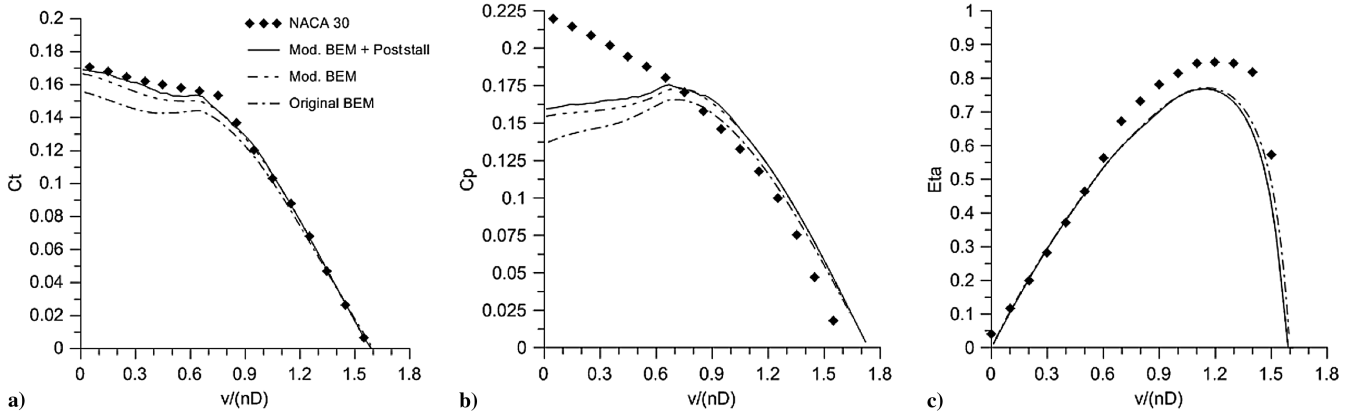

Fig. 11 Different formulations influence on the simulated propeller performance: a) thrust coefficient, b) power coefficient, and c) propeller efficiency.

efficiency is estimated at about a 10% lower value than the experiments. This is related to the overprediction for power coefficients at high advance ratios. One possible cause may be that the 3-D equilibrium condition still depends on the assumption of constant axial-induced velocity across the propeller disk. Comparing with JAVAPROP [50] and QPROP [28], JBLADE gives the best overall results.

Figure 13 shows the results of for the test case of NACA technical report 530 [48] for the reference propeller pitch angles of 30 deg (top), 40 deg (middle), and 50 deg (bottom) at 75% of the blade radius. Since

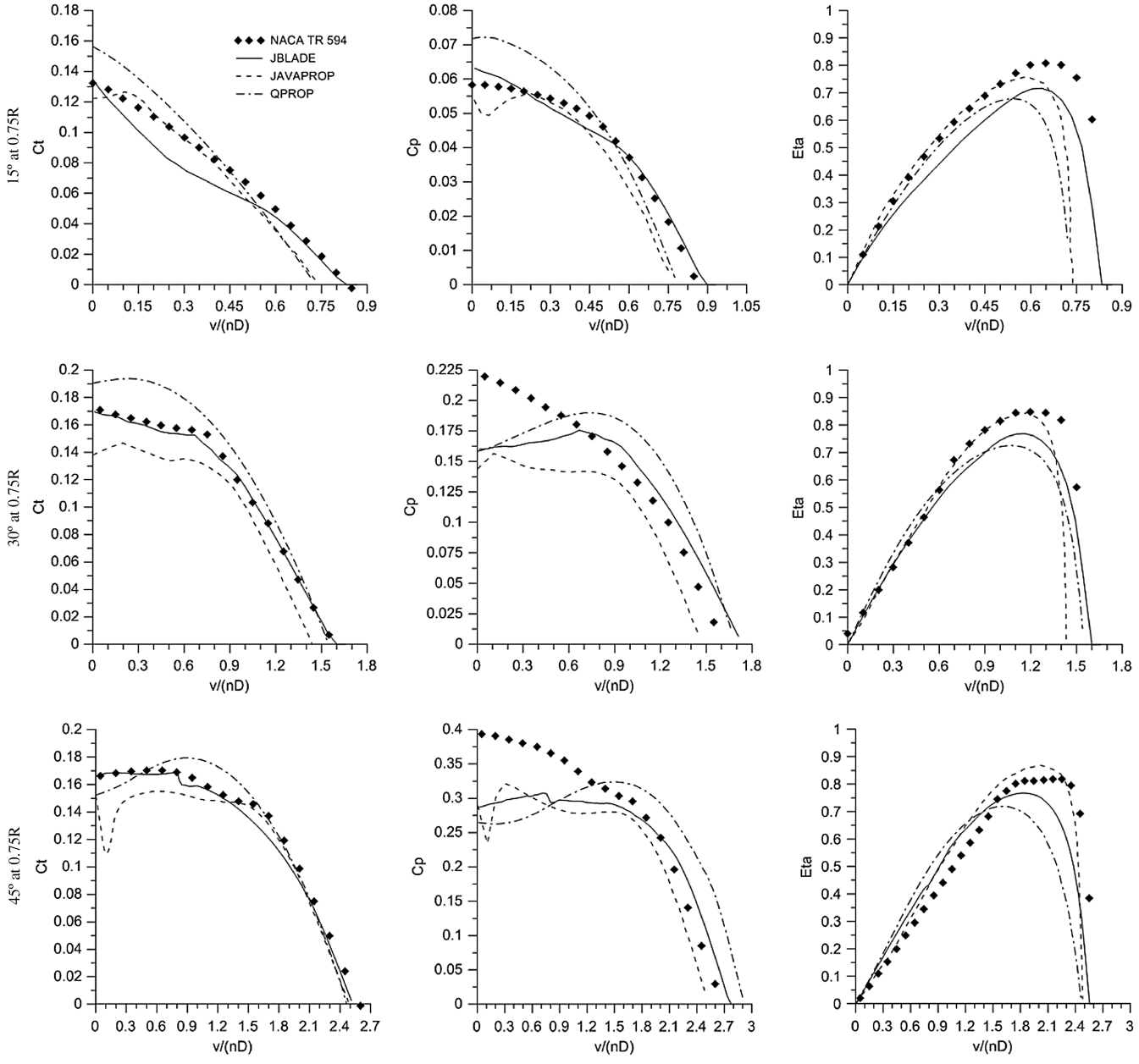

Fig. 12 Comparison between data predicted by JBLADE, QPROP [28], JAVAPROP [50], and data obtained from NACA Technical Report 594 [47].

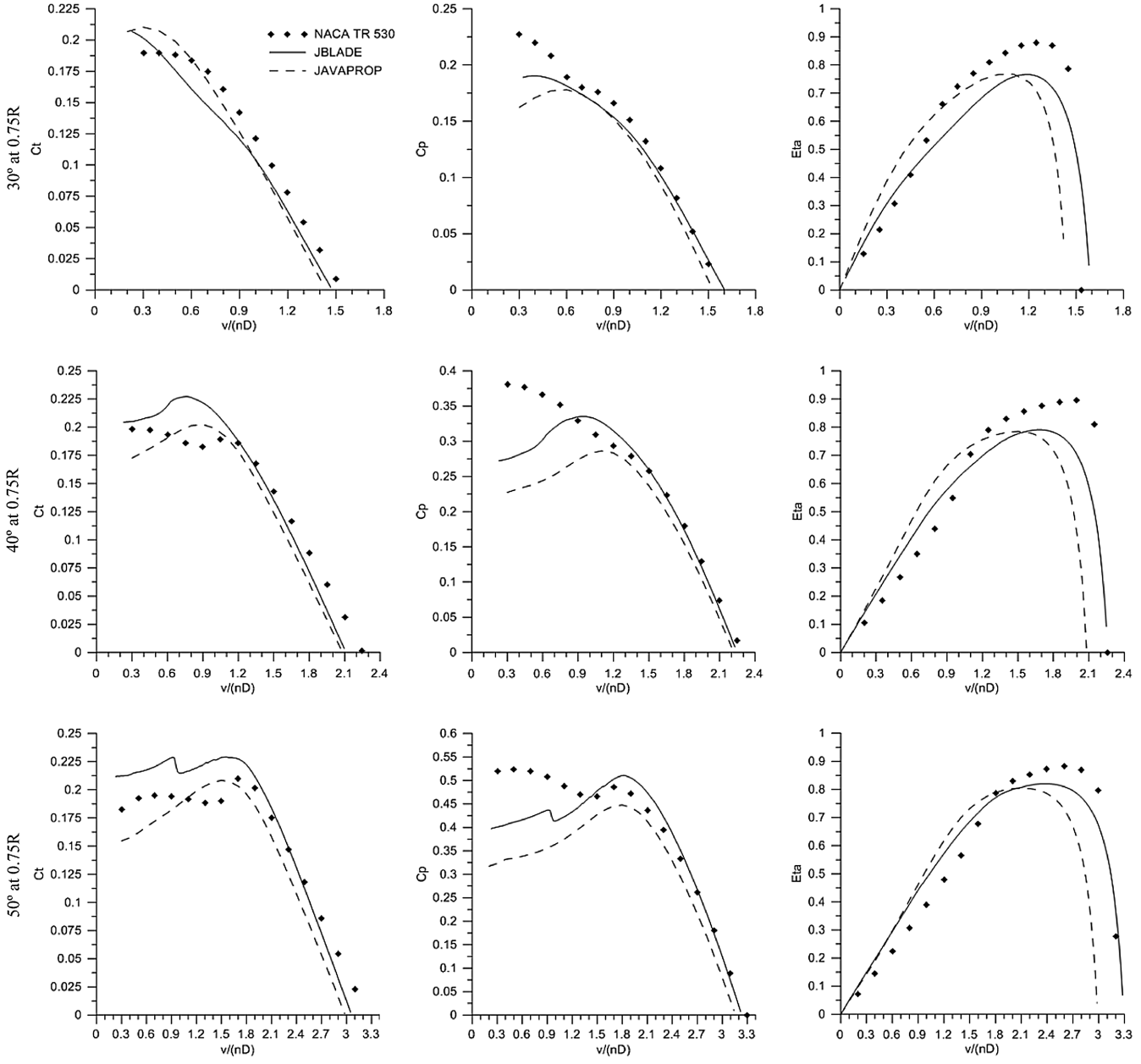

Fig. 13 Comparison between data predicted by JBLADE, JAVAPROP [50], and data obtained from NACA Technical Report 530 [48].

QPROP performed the worst in the first test case, only JAVAPROP was used for comparison with JBLADE in this second test case.

These results confirm that the power coefficient is underpredicted at low advance ratios, but contrary to what occurs in the previous test case, it is more closely estimated in the higher advance ratios. The thrust coefficient is significantly overestimated in the low-advance-ratios region, and it is slightly underpredicted in the higher-advance-ratios region, but the prediction is clearly closer to the experiments than that of JAVAPROP. Similar to the previous test case, the advance ratio for the maximum efficiency is correctly predicted, but the maximum efficiency is underestimated. Also, in this case, the advance ratio where the maximum efficiency occurs is correctly predicted. In this test case, this is related to the underprediction for thrust coefficients at high advance ratios. When compared with JAVAPROP, JBLADE confirms the best overall results.

IV. Conclusions

The JBLADE software proves to be useful for comparison of different propellers designs. The improvement of the classical BEM formulation with a 3-D flow equilibrium condition significantly improves the predictions for lower advance ratios with respect to other BEM codes. The correct modeling of the poststall airfoil characteristics was also found to play a major role in these low-advance-ratio performance predictions. This was achieved by studying a set of airfoil poststall characteristics in order to obtain a new correlation between the airfoil drag coefficient at 90 degr and the airfoil leading-edge radius. The proposed correlation proved to be reliable and can be used for all types of airfoils: both symmetric and asymmetric. The improvements in the method to extrapolate the drag coefficient polar, besides reducing the errors introduced by the user for not knowing what C_{D90} value to use, lead to significant improvements in the prediction of the propeller performance coefficients. The fitting of the correlation suggested by Timmer [36] was also improved and implemented, providing different options to extrapolate the drag coefficient for the full 360 deg of angle of attack. The new proposed models, after their implementation in JBLADE code, provided significant improvements on the prediction of the propeller performance.

Further improvement for the performance prediction at the low advance ratios might be achieved with high-fidelity CFD

simulations, given the suitability of turbulence models to obtain closer-to-real poststall airfoil characteristics. Nevertheless, computational fluid dynamics is more expensive and JBLADE allows a fast selection of the promising propeller geometry during an optimization procedure.

Acknowledgments

The present work was performed as part of Project Multibody Concept for Advanced Airship for Transport (reference no. 285602), supported by the European Union through the 7th Framework Programme. Part of the work was also supported by both the Center for Mechanical and Aerospace Sciences and Technologies and the Portuguese Foundation for Science and Technology (research unit no. 151).

References

[1] Wilson, J. R., "A New Era for Airships," *Aerospace America*, Vol. 42, No. 5, May 2004, pp. 27–31.

[2] Wang, X., Ma, Y., and Shan, X., "Modeling of Stratosphere Airship," *Advances in Theoretical and Applied Mechanics*, Vol. 2, No. 3, 2009, pp. 123–142.

[3] van Eaton, E. H., "Airships and the Modern Military," U.S. Army War College, Carlisle Barracks, Carlisle, PA, 1991, pp. 1–36.

[4] Liao, L., and Pasternak, I., "A Review of Airship Structural Research and Development," *Progress in Aerospace Sciences*, Vol. 45, Nos. 4–5, May–July 2009, pp. 83–96. doi:10.1016/j.paerosci.2009.03.001

[5] Morgado, J., Silvestre, M. Â. R., and Páscoa, J. C., "Parametric Study of a High Altitude Airship According to the Multi-Body Concept for Advanced Airship Transport—MAAT," *Proceedings of IV Conferência Nacional em Mecânica dos Fluidos, Termodinâmica e Energia*, Paper 90, LNEC, Lisboa, 2012.

[6] Dumas, A., Trancossi, M., Madonia, M., and Giuliani, I., "Multibody Advanced Airship for Transport," Soc. of Automotive Engineers TP-2011-01-2786, Warrendale, PA, 2011.

[7] Ilieva, G., Páscoa, J. C., Dumas, A., and Trancossi, M., "A Critical Review of Propulsion Concepts for Modern Airships," *Central European Journal of Engineering*, Vol. 2, No. 2, April 2012, pp. 189–200. doi:10.2478/s13531-011-0070-1

[8] Monk, J. S., "The Aerodynamic Design of an Optimised Propeller for a High Altitude Long Endurance UAV," *Proceedings of 23rd Congress of International Council of the Aeronautical Sciences*, ICAS Paper 2002-5.10.4, Pretoria, 2002.

[9] Rankine, W. M. J., "On the Mechanical Principles of the Action of the Propellers," *Transactions of the Institute of Naval Architects*, Vol. 6, No. 13, 1865, pp. 30–390.

[10] Froude, W., "On the Elementary Relation Between Pitch, Slip and Propulsive Efficiency," NASA TR-NASA-TM-X-61726, 1920.

[11] Drzewiecki, S., "Méthode Pour la Détermination des éléments Mécaniques des Propulseurs Hélicoïdaux," *Bulletin de L'Association Technique Maritime*, Vol. 3, No. 3, 1892, pp. 11–31.

[12] Betz, A., and Prandtl, L., "Schraubenpropeller mit Geringstem Energieverlust," *Göttinger Nachrichten*, Vol. 1919, 1919, pp. 193–217.

[13] Eppler, R., and Hepperle, M., "A Procedure for Propeller Design by Inverse Methods," *Proceedings of International Conference on Inverse Design Concepts in Engineering Sciences*, G.S. Dulikravich, Austin, TX, Oct. 1984, pp. 445–460.

[14] Glauert, H., "Airplane Propellers," *Aerodynamic Theory*, Dover, New York, 1963, pp. 251–268.

[15] Goldstein, S., "On the Vortex Theory of Screw Propellers," *Proceedings of the Royal Society of London, Series A: Mathematical, Physical and Engineering Sciences*, Vol. 123, No. 792, April 1929, pp. 440–465. doi:10.1098/rspa.1929.0078

[16] Theodorsen, T., *Theory of Propellers*, McGraw–Hill, New York, 1948, pp. 1–168.

[17] Larrabee, E. E., "Practical Design of Minimum Induced Loss Propellers," Soc. of Automotive Engineers TP-790585, Warrendale, PA, 1979.

[18] Adkins, C. N., and Liebeck, R. H., "Design of Optimum Propellers," *Journal of Propulsion and Power*, Vol. 10, No. 5, 1994, pp. 676–682. doi:10.2514/3.23779

[19] Tangler, J. L., and Ostowari, C., "Horizontal Axis Wind Turbine Post Stall Airfoil Characteristics Synthesization," *DOE/NASA Wind Turbine Technology Workshop*, Paper DE91002198, 1984.

[20] Wald, Q., "The Aerodynamics of Propellers," *Progress in Aerospace Sciences*, Vol. 42, No. 2, 2006, pp. 85–128. doi:10.1016/j.paerosci.2006.04.001

[21] Montgomerie, B., "Drag Coefficient Distribution on a Wing at 90 Degrees to the Wind," The Energy Research Center of the Netherlands (ECN) ECN-95-061, Amesterdam, 1996.

[22] Lindenburg, C., "Aerodynamic Airfoil Coefficients at Large Angeles of Attrak," *Proceedings of Annual IEA Symposyum on the Aerodynamics of Wind Turbines*, Paper ECN-RX-01-004, Golden, CO, Dec. 2000.

[23] Ostowari, C., and Naik, D., "Post Stall Studies of Untwisted Varying Aspect Ratio Blades with a NACA 44XX Series Airfoil Sections—Part II," *Wind Engineering*, Vol. 9, No. 3, 1985, pp. 149–164.

[24] Snel, H., Houwink, R., and Bosschers, J., "Sectional Prediction of Lift Coefficients on Rotating Wind Turbine Blades in Stall," The Energy Research Center of the Netherlands (ECN) ECN-C-93-052, Amesterdam, 1994.

[25] Hand, M. M., Simms, D. A., Fingersh, L. J., Jager, D. W., Cotrell, J. R., Schreck, S., and Larwood, S. M., "Unsteady Aerodynamics Experiment Phase VI: Wind Tunnel Test Configurations and Available Data Campaigns," National Renewable Energy Lab. TR-500-29955, Golden, CO, 2001.

[26] Lindenburg, C., "Investigation into Rotor Blade Aerodynamics Analysis of the Stationary Measurements on the UAE Phase-VI Rotor in the NASA-Ames Wind Tunnel," The Energy Research Center of the Netherlands (ECN) ECN-C-03-025, Amesterdam, 2003.

[27] Tangler, J. L., "The Nebulous Art of Using Wind-Tunnel Airfoil Data for Predicting Rotor Performance: Preprint," *Proceddings of ASME 2002 Wind Energy Symposium*, American Soc. of Mechanical Engineers, Fairfield, NJ, 2002, pp. 190–196. doi:10.1115/WIND2002-40

[28] Drela, M., "QPROP Formulation," 2006, http://web.mit.edu/drela/Public/web/qprop/qprop_theory.pdf [retrieved 25 Oct. 2013].

[29] Saravanamuttoo, H., Rogers, G., and Cohen, H., *Gas Turbine Theory*, 4th ed., Longman Group Ltd., London, 1996, pp. 169–179.

[30] Ananda, G., *UIUC Propeller Database* [database], Aerospace Engineering, Univ. of Illinois Champaign, IL, http://aerospace.illinois.edu/m-selig/props/propDB.html [retrieved 25 Feb. 2014].

[31] *ANSYS FLUENT Theory Guide*, Ansys. Inc., Ann Arbor, MI, 2010.

[32] Menter, F., Ferreira, J. C., Esch, T., and Konno, B., "The SST Turbulence Model with Improved Wall Treatment for Heat Transfer Predictions in Gas Turbines," *Proceedings of the International Gas Turbine Congress*, Paper IGTC2003-TS-059, Tokyo, 2003, pp. 2–7.

[33] Gault, D., "A Correlation of Low Speed Airfoil Section Stalling Characteristics with Reynolds Number and Airfoil Geometry," NACA TN-3963, March 1957.

[34] Montgomerie, B., "Methods for Root Effects, Tip Effects and Extending the Angle of Attack Range to ± 180 deg, with Application to Aerodynamics for Blades on Wind Turbines and Propellers," Swedish Defence Research Agency FOI-R-1305-SE, Stockholm, June 2004.

[35] Abbott, I., von Doenhoff, A., and Stivers, L., "Summary of Airfoil Data," NACA TR-824, 1945.

[36] Timmer, W. A., "Aerodynamic Characteristics of Wind Turbine Blade Airfoils at High Angles-of-Attack," *Proceedings of TORQUE 2010: The Science of Making Torque from Wind*, Crete, 2010, pp. 71–78.

[37] Massini, G., Rossi, E., and D'Angelo, S., "Wind Tunnel Measurements of Aerodynamics Coefficients of Asymmetrical Airfoil Sections for Wind Turbines Blades Extended to High Angles of Attack," *Proceedings of European Wind Energy Conference*, Paper EN3W/0018/I-JB, H.S. Stephens & Associates, Herning, 1988, pp. 241–245.

[38] Miley, S., *A Catalog of Low Reynolds Number Airfoil Data for Wind Turbine Applications*, Dept. of Aerospace Engineering Texas A&M Univ., College Station, TX, 1982, pp. 1–48.

[39] Ostowari, C., and Naik, D., "Post Stall Studies of Untwisted Varying Aspect Ratio Blades with a NACA 4415 Series Airfoil Sections—Part I," *Wind Engineering*, Vol. 8, No. 3, 1984, pp. 176–194.

[40] Silvestre, M. A., Morgado, J. P., and Pascoa, J., "JBLADE: A Propeller Design and Analysis Code," *2013 International Powered Lift Conference*, AIAA Paper 2013-4220, 2013. doi:10.2514/6.2013-4220

[41] Corrigan, J., and Schillings, J., "Empirical Model for Blade Stall Delay Due to Rotation," *Proceedings of the American Helicopter Society Aeromechanics Specialists*, Paper 8.4, San Francisco, 1994, pp. 1–15.

[42] "Qt Project," Software Version: Qt Creator 2.4.1, Digia PLC, Helsinki, 2013, http://qt-project.org/ [retrieved 18 Feb. 2014].

[43] Marten, D., Wendler, J., Pechlivanoglou, G., Nayeri, C. N., and Paschereit, C. O., "QBLADE: An Open Source Tool for Design and Simulation of Horizontal and Vertical Axis Wind Turbines," *International Journal of Emerging Technologies and Advanced Engineering*, Vol. 3, No. 3, Feb. 2013, pp. 264–269.

[44] Marten, D., and Wendler, J., "QBlade Guidelines v0.6," Technical Univ. of Berlin, Berlin, 2013.

[45] Deperrois, A., *Analysis of Foils and Wings Operating at Low Reynolds Numbers — Guidelines for XFLR5 v6.03*, 2011, http://www.xflr5.com/xflr5.htm [retrieved 3 Nov. 2013].

[46] Drela, M., "XFOIL—An Analysis and Design System for Low Reynolds Number Airfoils," *Low Reynolds Number Aerodynamics Lecture Notes in Engineering*, Vol. 54, Springer, Berlin, 1989, pp. 1–12.

[47] Theodorsen, T., Stickle, G. W., and Brevoort, M. J., "Characteristics of Six Propellers Including the High-Speed Range," NACA TR-594, 1937.

[48] Gray, W., "Wind-Tunnel Tests of Two Hamilton Standard Propellers Embodying Clark Y and Naca 16-Series Blade Sections," NACA TR-530, 1941.

[49] Selig, M. S., and Guglielmo, J. J., "High-Lift Low Reynolds Number Airfoil Design," *Journal of Aircraft*, Vol. 34, No. 1, Jan. 1997, pp. 72–79. doi:10.2514/2.2137

[50] Hepperle, M., "JavaProp—Design and Analysis of Propellers—User's Guide," 2010, http://www.mh-aerotools.de/airfoils/javaprop.htm [retrieved 4 Nov. 2013].

F. Liu
Associate Editor